LAWRENCE
LIVERMORE
NATIONAL
LABORATORY

UCRL-JRNL-236118

Strength in numbers: Probing and understanding intermolecular bonding with Chemical Force Microscopy

A. Noy

November 2, 2007

Scanning

Disclaimer

Strength in numbers:

Probing and understanding intermolecular bonding with Chemical Force Microscopy

Aleksandr Noy

Chemistry, Materials, Energy, and Life Sciences Directorate,
Lawrence Livermore National Laboratory, Livermore, CA 94550

School of Natural Sciences,
University of California Merced, Merced, CA 95344

E-mail: *noy1@llnl.gov; anoy@ucmerced.edu*

Summary.

Scanning probe microscopy (SPM) provided researchers with a simple, intuitive, and versatile tool for probing intermolecular interactions using SPM probes functionalized with distinct chemical functionalities. Chemical force microscopy was developed as a way to probe and map these interactions in a rational and systematic way. But does the rupture strength of a bond measured in these experiments provide the definitive and useful information about the interaction? We show that the answer to this question is closely linked to understanding the fundamental physics of bond rupture under an external loading force. Even a simple model shows that bond rupture can proceed in a variety of different regimes. We discuss the approaches for extracting quantitative information about the interaction from these experiments and show that even though the measured rupture force is almost never unique for a given bond, force spectroscopy measurements can still determine the essential interaction parameters.

SPM as a tool for probing intermolecular interactions.

Intermolecular bonding is one of the most fundamental and the ubiquitous concepts in physical chemistry. It is virtually impossible to describe any of the condensed matter phenomena, whether it is vapor condensation, stress fracture, molecular recognition, or friction and wear, without invoking the concept of intermolecular bonding. Indeed, in most chemical and biological systems simple pair-wise interactions between individual molecules and molecular assemblies combine to produce complicated structures and cause the driving forces that shape our world. This picture of the world driven by chemical interactions has always enticed the scientists to

adopt a structural engineer's view of condensed matter phenomena: if we can reconstruct the forces involved in each of these pair-wise interactions, then we can build a realistic model of complex processes. Notably, recent advances in computing power and the increasing sophistication of modern molecular dynamics modeling methods have began to realize this vision, (Freddolino et al., 2006). However, it is important to realize that the accuracy of these models would always dependent on the accuracy of their input; in other words, the utility of these models depends on our knowledge of the basic intermolecular interactions.

How can we probe the intermolecular interactions? Again, the "structural engineering" view provides a deceptively simple concept: if only we could grab the interacting molecules with some "handles," pull them apart, and measure the forces it takes to break the bond, then we would have a simple, direct, and unambiguous way to characterize the interaction strength. This simple experiment has remained an impossible dream up until the advent of modern single molecule manipulation techniques. Notably, shortly after the invention of the scanning probe microscopy researchers realized that these instruments could be used not only to map the surfaces, but also to probe nanoscale interactions ((Binnig et al., 1986; Burnham et al., 1991; Mate et al., 1987; Meyer et al., 1988)). Atomic force microscope (AFM) is a ubiquitous instrument in today's nanotechnology laboratories, and it is not necessary to describe it in detail; suffice to say that it uses a sharp tip mounted on the end of a microfabricated flexible cantilever to probe the sample mounted on a piezoelectric scanner that controls the sample position in all three spatial dimension (Figure 1A). An AFM possesses several key advantages for probing forces on the small scale using the microscope's cantilever as a miniature force sensing spring. First, piezoelectric scanners allows angstrom-level vertical resolution of the probe tip position that is necessary to study these interactions on the relevant length scales. Second, the sharpness of the probe tip makes it a truly local probe, giving researchers the ability to address interactions close to the single molecule level. Third, miniaturized microfabricated AFM cantilevers (Albrecht et al., 1990) provide the low stiffness probes necessary to measure molecular interactions. Characteristic potential energy gradients of intermolecular interactions range from 10^{-12}N to 10^{-7}N (Israelachvili, 1992), which corresponds to the range of useful spring constants of 0.01-1 N/m, given the typical AFM deflection range of 0.1-100 nm. Fortunately, this range of spring constants overlaps very well with the range of springs constants available for commercial AFM probes today.

From the point of view of force measuring an AFM can be described as a simple system that consists of two elastic elements connected in series (Figure 1B). One of these elements corresponds to an intermolecular bond, and another to the cantilever spring or, as often is common in the biological interactions measurements, to a combination of the stiffness of the AFM cantilever and the stiffness of polymer linkers that attach the interacting species to the probe and sample surfaces (in those cases the probing spring can no longer be described by a harmonic Hookean potential, but instead corresponds roughly to a semiharmonic potential; for detailed discussion see (Sulchek et al., 2007)). In a typical measurement the piezo scanner stretches this construct until the chemical bond ruptures. For the serial connection the force acting on the cantilever spring is equal to the force acting on the bond, therefore the cantilever

deflection at the rupture point can provide an accurate measure of the rupture force. In practice, the measurement involves operating the AFM instrument in a "force curve" cycle (Figure 1C) where the scanner repeatedly brings the probe tip in and out of contact with the surface. Bond rupture causes a sharp jump in the cantilever deflection and the magnitude of this jump in the force curve corresponds to the rupture force value.

Chemical force microscopy.

Despite the conceptual simplicity of a force curve measurement the utility of the standard AFM setup for measuring specific forces is severely limited by the unknown chemical composition of the AFM tip. Standard silicon and silicon nitride probes present a poorly defined chemical interface and more often than not pick up contaminations during the measurements. A concept of Chemical Force Microscopy (CFM), introduced by Lieber and coworkers (Noy et al., 1995), replaces this poorly characterized interface with a well-defined system produced by deliberate functionalization of the tip and sample surfaces (Figure 2). These modifications in effect transform AFM from a tool for measuring ill-defined interactions of silicon probes with surfaces into a tool for measuring specific chemical interactions. Careful design of the probe coating also prevents contaminations, controls the number of interacting molecules, and even separates different types of interaction. Researchers have used chemically-modified AFM probes for a number of applications including adhesion and friction measurements, as well as high-resolution imaging. CFM progress and key results have been the subject of several detailed reviews (Noy et al., 1997; Noy et al., 2007; Vezenov et al., 2005), therefore I will not repeat them here.

What does a CFM experiment measure? A naïve point of view attributes the measured rupture force to the maximum gradient of the intermolecular interaction potential; however, it is easy to point out the flaws of this approach: (i) it does not include any energy dissipation effects, and (ii) it does not take into account any thermal fluctuations. Indeed, even the early CFM measurements provided strong hints that this approach was not entirely accurate. For example, interaction forces measured by two different research groups using probe tips and samples modified with COOH chemical functionalities differed almost by an order of magnitude, 2.3nN (Noy et al., 1995) vs. 0.27 nN (Sinniah et al., 1996). The interpretation of the CFM experiments based on the Johnson, Kendall, and Roberts model of interfacial contact mechanics (Johnson et al., 1971) has put CFM on a solid quantitative footing (Noy et al., 1997) and revealed how rupture forces scale with the probe size and tip-sample contact area for these experiments (Skulason et al., 2000; Skulason et al., 2002). Puzzlingly, in the case of the two studies mentioned previously even accounting for the differences in reported probe radii was not sufficient to explain the differences in the measured rupture forces.

To understand these effects we need to notice that even the sophisticated contact mechanics model does not take into account the two factors mentioned in the previous paragraph: energy dissipation and thermal fluctuations. To understand the key role played by these two parameters in determining the experimentally-measured rupture forces we need to consider the basic physics of the bond rupture under an external loading force.

Pulling on a chemical bond with a spring: a physical chemist's view.

An ideal AFM experiments would measure an equilibrium force profile, which is a derivative of a one-dimensional slice of the potential energy surface along a reaction coordinate defined by the pulling direction. In the simplest case, we can represent the tip-sample interaction with a single-well potential, and assume a parabolic potential of a Hookean spring for the cantilever (Figure 3). The overall potential of the system, which determines equilibrium position of the cantilever, is then a sum of these two potentials (Figure 3). A simple analysis shows that depending on the cantilever stiffness the system can behave in two very different ways: (i) For stiff cantilevers, the spring potential is so steep that it prevents formation of any secondary minima at all separations. Therefore, as the cantilever approaches and retracts from the surface, the forward and reverse traces coincide, and the probe simply traces the entire potential energy well. (ii) When the cantilever spring is relatively soft, the parabolic potential is shallow and a secondary minimum can emerge at certain separations, causing a sudden jump of the cantilever away from the surface during retraction. This instability precludes the probe tip from sampling a large part of the potential energy profile. Steep potential energy gradients typical of the interaction forces and the limitations imposed by the AFM sensitivity and noise levels make the situation (ii) overwhelmingly prevalent in the CFM measurements. Therefore, to understand the measurement we need to consider the kinetics of the transition from the bound state corresponding to the interaction potential minimum into an unbound state corresponding to the secondary minimum formed by the potential of the loading spring. It is reasonable to assume that the loading force changes much slower that frequency of the thermal fluctuations; therefore the unbinding transition is driven by thermal fluctuations and the role of the external force is limited to changing the overall potential energy landscape of the system. (Note that the loading force typically increases linearly in an AFM experiment). In other words, force-induced bond rupture in the atomic force microscope is simply a *transition from the bound state into an unbound state over a potential energy surface that is constantly modified by the potential of the loading spring.*

In the most general case, the dynamics of this two-well system involves two elementary first order processes, unbinding and rebinding, with each process characterized by a rate constant.

$$\begin{aligned} Bound &\xrightarrow{k_{unb}} Unbound \\ Bound &\xleftarrow{k_{reb}} Unbound \end{aligned} \qquad (1)$$

As Bell showed in his pioneering work [43], loading the system in the direction of unbound state lowers the barrier to unbinding and simultaneously raises the barrier to rebinding. Consequently, loading leads to the amplification of unbinding rate constant, k_{unb}, and retardation of the rebinding rate constant, k_{reb}:

$$k_{unb} = k_{unb}^{0} \cdot e^{\frac{F \cdot x_{\beta}^{f}}{k_B T}} \qquad (2)$$

$$k_{reb} = k_{reb}^{0} \cdot e^{\frac{-F \cdot x_{\beta}^{r}}{k_B T}} \qquad (3)$$

where x_{β}^{f} denotes the distance to the transition state from the bottom of the primary well and x_{β}^{r} is the distance to the transition state from the bottom of the secondary, cantilever-induced potential well. As the next sections will show, these two simple equations describe a surprisingly reach universe of unbinding dynamics.

A simple qualitative analysis shows that the unbinding transition in this system can happen in two different regimes, as determined by the unbinding and rebinding rates. Under slow loading conditions, the unbinding proceeds as an equilibrium process and the force necessary to break the bond is simply determined by the energy difference between bound and unbound states. Note that the exponential retardation of the rebinding rate (Equation 3) places a rather restrictive condition on the range of loading rates that could cause this behavior. Alternatively, if the loading rate is comparable with the rate of at least one of the processes described by the Equation 1, the system never reaches equilibrium before the bond breaks. It is clear even from this simplistic description that the measured unbinding force is very dependent on the way the bond is loaded. Thus we can use the loading history of the bond to define three general regimes of the bond rupture:

1. Non-equilibrium unbinding under fast loading conditions.
2. Near-equilibrium unbinding under slow loading.
3. Intermediate loading regime where the rebinding is nether completely suppressed nor strong enough to play a major role.

I now consider the interpretation of the CFM measurements representing each of these regimes separately.

Fast loading regime: Non-equilibrium unbinding.

As we discussed before, non-equilibrium unbinding typically occurs when strong chemical bonds are stretched fast with soft springs which place the probe-induced energy minimum far away from the transition state (consider the effect of this situation on the Equation 3!). Note that use of flexible polymer linker "handles" common in the CFM measurements using biological targets has an even more dramatic effect on the Equation 3 as it places the unbound state very far from the energy barrier and in effect eliminates any possibility for the rebinding process. Rupture force kinetics in this situation was first developed by Evans in a series of publications that established the kinetic approach to the non-equilibrium bond rupture as *dynamic force spectroscopy* (Evans, 1999; Evans et al., 1997; Merkel et al., 1999).

To simplify the analysis we can postulate that the unbound state is located infinitely far away on the reaction coordinate and that we can approximate the potential of the AFM cantilever by a linear function instead of a parabola. Note that this model completely neglects rebinding;

therefore it must postulate that thermal fluctuations will eventually break the bond even in absence of external force. Thus, every bond is characterized by a finite lifetime, or a natural kinetic off-rate k_{off}. Loading the bond exponentially amplifies the escape rate (Equation 2), and the system acquires a higher probability to reach the top of the barrier. Qualitatively, at lower applied forces the barrier still remains too high for the thermally-activated transition to occur, and at higher applied forces the transition has most likely happened already. A peculiar consequence of this kinetics is that most of the unbinding events happen in a fairly narrow range of the applied forces, which ultimately defines the bond strength that we register in the experiment. Kramers' theory of thermally-assisted barrier crossing in liquids provides an analytical expression for the measured rupture force (Evans et al., 1997). For the constant loading rate, r_f, the measured binding force in the non-equilibrium rupture regime is given by:

They obtained the following expression for the pull-off force (Evans, 1999):

$$f_{pull-off} = \frac{k_B T}{x_\beta} \ln\left(\frac{r_f}{r_0}\right) \tag{4}$$

where r_0 is defined as:

$$r_0 = \frac{k_B T}{x_\beta} \cdot k_{off} \tag{5}$$

and x_β is the distance to the transition state (equivalent to $x_{\beta f}$ in the Equation 2). Immediately, we can see from Equation 4 that the pull-off force increases logarithmically as the loading rate r_f increases. Thus, bond strength can vary quite significantly over a wide range of loading rates. Moreover, measuring the rupture force as a function of the loading rate (often called a dynamic force spectrum) provides a simple way to obtain value of the distance to the potential barrier, x_β, and the kinetic off-rate k_{off}.

Recent literature contains many examples of the use of dynamic force spectroscopy to determine to probe energy landscape parameters for a number of interactions between biological and chemical species, such as DNA (Pope et al., 2001; Strunz et al., 1999), RNA (Green et al., 2004), proteins and ligands (Patel et al., 2004; Williams et al., 2003), and enzymes and drugs (Rigby-Singleton et al., 2002). For example, the dynamic force spectrum of the interactions between an cancer marker peptide MUC1 and an antibody fragment specific to MUC1 (Figure 4) shows the linear behavior predicted by the Equation 4 and provides a value of the distance to the transition state that closely matches the value predicted from the MD simulations, (Sulchek et al., 2005). Moreover, the kinetic off-rate for this interaction measured in this study correlated with the k_{off} value determined from the SPR measurements. The utility of non-equilibrium force spectroscopy (i.e. dynamic force spectroscopy) for routine determination of the kinetic off-rates on a single molecule level is still under investigation, however it is clear that it has a unique advantage in at

least one area- measurement of extremely tight binding interactions that are characterized by very long off-times. In this case the exponential amplification of unbinding kinetics due to the applied force is critical for enabling researchers to observe the unbinding events on a reasonable timescale.

Non-equilibrium force spectroscopy is useful for studying not only single, but also multiple bonds. In those system the researchers face an additional challenge of determining the exact number of the interacting species. The detailed description of the procedures for accomplishing this goal are beyond the scope of this article, therefore briefly naming some of them will suffice. Even though contact mechanics models grossly oversimplify the physics of nanoscale bond rupture, they can be useful for estimating the contact area (Luan et al., 2005) and the number of interacting groups. For measurements of the interactions of biological molecules attached to the flexible tethers, the elastic properties of the tethers could provide an independent means of determining the number of interacting molecules (Sulchek et al., 2006).

Slow loading regime: Near-equilibrium unbinding.

At first glance slow loading should lead to a rather simple bond rupture behavior: the magnitude of the measured rupture force should be determined solely by the thermal equilibrium between the bound and unbound states and the kinetics factors should not play a significant role. Indeed, we expect that as the loading rate drops, the characteristic logarithmic dependence of rupture force on the loading rate will vanish and the rupture behavior will transition to the regime where the measured bond strength would be independent of the loading rate (see Figure 5). This notion of the equilibrium unbinding then gives a glimpse of hope to define a meaningful value of the bond rupture force as an objective measure of the bond strength. The origin of the plateau in the force spectrum could also be understood using the following argument: If we consider the shape of the combined energy landscape of the bond and the cantilever, we can see that it is virtually impossible to observe a rupture event at zero applied force because the outer part of the harmonic probe potential prevents the complete dissociation of the bond! Dissociation becomes possible only when the probe moves away by a sufficient amount to define a secondary minimum on the potential energy surface. Thus bond rupture could not happen until the applied force reaches a threshold value which then defines the lower limit to the measured rupture forces and consequently the force plateau value. Indeed, rupture forces measured in the CFM experiments confirm this prediction and show a distinct plateau in the force spectrum at slow loading rates (Figure 6A).

Unfortunately, these arguments also point out the main complication of near-equilibrium rupture: unlike spontaneous unbinding, bond rupture in the force spectroscopy experiment is controlled by the potential of the bond *and* the potential of the AFM cantilever spring (i.e. by the potential of the unbound state). It is clear from the diagram on the Figure 3 that different probe stiffness changes the shape of the potential energy surface and must have a significant effect on the transition probabilities defined by the Eq. 2 and 3. Thus we arrive at a puzzling realization: *the magnitude of the measured equilibrium unbinding force must depend on the stiffness of the*

probe used to measure this force! This behavior was first mentioned briefly by Evans early on (Evans, 2001), and has remained virtually unexplored until very recently (Friddle et al., 2007b). Indeed, a detailed analysis of the rupture transition shows that at slow loading approaching the near-equilibrium unbinding regime the measured rupture force will be given by (Friddle et al., 2007b):

$$f_{eq} = \sqrt{2k_s \cdot [U_0 - k_B T \ln(\omega_b/\omega_u)]} \quad (6)$$

where k_s is the cantilever spring constant and ω_b and ω_u are the characteristic frequencies of the bound and unbound state. Note that the second term in the Equation 6, $[k_B T \ln(\omega_b/\omega_u)]$ corresponds to the entropy difference between the bound and unbound state, which leads to a very simple conclusion:

$$f_{eq} = \sqrt{2k_s \cdot [U_0 - \Delta S]} \approx \sqrt{2k_s \cdot \Delta G} \quad (7)$$

The most important prediction from the equation (7) is that the rupture force measured in the near-equilibrium regime is proportional to the square root of the stiffness of the loading cantilever, and that the proportionality coefficient depends only on the free energy difference between the bound and unbound states. Computer simulations (Figure 5) and the experimental measurements (Figure 6B) confirm this prediction (Friddle et al., 2007b). Moreover, an estimate of the energy of a hydrogen bond between two COOH groups in ethanol using this method provides a value of 5.7kJ/mole (Friddle et al., 2007b), which compares favorably with a thermodynamic estimate of 5.4 kJ/mol (van der Spoel et al., 2006). What can we learn from the near-equilibrium measurements? Although they cannot not provide an objective, measurement-independent rupture force value, they nevertheless can determine the free energy of a bond by measuring the rupture forces using cantilevers of different stiffness!

Full kinetic description of bond rupture.

Finally, we need to address a question of interpreting the force spectroscopy measurements in cases where a full force spectrum is not known is difficult to determine. In these cases the experimenters need to rely on the full kinetic description of the force spectroscopy experiments (Dudko et al., 2003; Heymann et al., 2000). These models are also useful in describing bond rupture in the cases that fall between the two loading regimes that we discussed in the previous sections. Not surprisingly, using these universal models brings significant trade-offs: the equations describing the rupture kinetics are not nearly as simple and often the researchers need to resort to using numerical solutions instead of analytical solutions. These models also tend to depend on a large number of parameters that could complicate the fitting procedure and reduce the precision of the results. Nevertheless, full kinetic models still have significant utility for the interpretation of force spectroscopy experiments. Noy and coworkers used a full kinetic formalism developed by Urbakh and colleagues (Dudko et al., 2003) to analyze the result of the experiments that measured the interactions of single functional groups with carbon nanotube sidewall surfaces (Friddle et al., 2007a). These measurements exploited very high curvature of the

carbon nanotube surface to shrink the tip-sample contact area down to the size of a single functional group. This ability to repeatedly achieve single functional group contact allowed researchers to observe and quantify the spread in the measured rupture force values caused by thermal fluctuations. Moreover, small scale of the interactions and the relative simplicity of the system provided a unique opportunity to compare the experimental measurements with the results of *ab initio* computer simulations of the interactions (Figure 7).

Urbakh and colleagues's formalism predicts the rupture force distribution based on the shape of the interaction energy profile along the pulling coordinate(Dudko et al., 2003) as:

$$P(F) = P_0 \varepsilon^{1/2} \exp\left\{ -\frac{U_c}{k_B T} \varepsilon^{3/2} - \frac{k_B T \omega_c^2 m F_c}{U_c 3\pi \gamma k v} e^{-\frac{U_c}{k_B T}\varepsilon^{3/2}} \right\}, \qquad (8)$$

where k and v are respectively the cantilever spring constant and pulling velocity and γ is the damping coefficient of the system. The parameters U_c and ω_c respectively are the characteristic energy and oscillation frequency of the unperturbed bond; m is the effective particle mass, ε=1-F/F_c is the reduced bias relative to the critical force F_c at which the energy barrier vanishes, and P_0 is a normalization constant. Remarkably, the rupture force distributions determined using Equation 7 and interactions potentials calculated from *ab initio* simulations closely reproduced the measured distributions for three different functional groups (Figure 7).

These results also reveal an interesting and important feature of molecular-scale interactions: the important role played by the intermolecular damping in determining the rupture kinetics. Notice that the forces measured for probes functionalized with n-butylsilane and octadecylsilane (Figure 7B,C) were not identical despite the probes terminating with the same functional groups In this case the detailed analysis of the force measurements shows that the damping coefficients determined for the probes functionalized with short silanes, $1.34 \cdot 10^{-4}$ kg/s, matches the damping coefficients measured for an AFM cantilever in close proximity to a surface. Connecting the functional group to the cantilever with a much longer linker decreases the effective damping coefficient to $0.30 \cdot 10^{-4}$ kg/s. This smaller damping coefficient increases the kinetic unbinding rate, and results in a smaller measured rupture forces. This example shows the utility of force spectroscopy measurements as a unique tool for understanding molecular-scale details of nanoscale interactions.

Outlook: Can we learn anything from Chemical Force Microscopy experiments?

At the first glance, quantitative analysis of the force spectroscopy experiments produces mildly frustrating conclusions: the measured forces are never unique and almost always are highly dependent on the context of the experiment. In fact, the analysis shows that for a given interaction potential a suitable choice of a probing cantilever stiffness can produce any value of the rupture force at a given loading rate as long as that rupture force-rate combination lies within

the allowed region in the force spectrum (Figure 5, unshaded region). This analysis completely shatters the naïve notion of using the bond rupture force as a means of measuring and comparing bond strength. Instead the past decade of chemical force microscopy development (and force spectroscopy development in general) has brought into focus the central role that the fundamental thermodynamic and kinetic parameters of the bond, such as the bond rupture free energy, kinetic off-rate, and the distance to the barrier, play in determining the rupture kinetics. Once the paradigm is shifted from simply measuring the bond strength to using force-induced bond rupture measurements to probe these fundamental thermodynamic parameters, the utility of the force spectroscopy measurements becomes much clearer.

As the previous sections have shown, chemical force microscopy measurements could provide a wealth of data on intermolecular interactions, but getting these data requires careful planning of the experiment, careful attention to the measurement details, choosing the proper cantilever stiffness and loading rate range, and choosing the right quantitative framework for interpreting the data. Only then Chemical Force Microscopy can fulfill its original promise- to become a versatile nanoscale tool for rigorous quantitative analysis of intermolecular interactions.

Acknowledgments.

A.N. acknowledges support from NSF NIRT CBET-0709090 and Office of Basic Energy Science (BES), Division of Materials Science and Engineering. A.N. thanks Dr. R. W. Friddle for calculating the distributions depicted on the Figure 3. Parts of this work were performed under the auspices of the U.S. Department of Energy by Lawrence Livermore National Laboratory under Contract DE-AC52-07NA27344.

References:

Albrecht, T. R., S. Akamine, T. E. Carver and C. F. Quate: Microfabrication of cantilever styli for the atomic force microscope. J. Vac. Sci. Technol. A, Vac. Surf. Films **8**, 3386-96 (1990).

Binnig, G., C. F. Quate and C. Gerber: Atomic force microscope. Phys. Rev. Lett. **56**, 930-3 (1986).

Burnham, N. A., R. J. Colton and H. M. Pollock: Interpretation issues in force microscopy. J. Vac. Sci. Technol. A, Vac. Surf. Films **9**, 2548-56 (1991).

Dudko, O. K., A. E. Filippov, J. Klafter and M. Urbakh: Beyond the conventional description of dynamic force spectroscopy of adhesion bonds. Proc. Natl. Acad. Sci. USA **100**, 11378-11381 (2003).

Evans, E.: Energy landscapes of biomolecular adhesion and receptor anchoring at interfaces explored with dynamic force spectroscopy. Farad. Disc. 1-16 (1999).

Evans, E.: Probing the Relation Between Force—Lifetime and Chemistry in Single Molecular Bonds. Ann. Rev. Biophys. Biomol. Struct. **30**, 105-128 (2001).

Evans, E. and K. Ritchie: Dynamic strength of molecular adhesion bonds. Biophys. J. **72**, 1541-1555 (1997).

Freddolino, P. L., A. S. Arkhipov, S. B. Larson, A. McPherson and K. Schulten: Molecular Dynamics Simulations of the Complete Satellite Tobacco Mosaic Virus. Structure **14**, 437-449 (2006).

Friddle, R., M. Le Mieux, G. Cicero, A. Artyukhin, V. Tsukruk, J. Grossman, G. Galli and A. Noy: Single functional group interactions with sidewalls of individual carbon nanotubes. Nature Nanotechnology, AOP, 10.1038/nnano.2007.334 (2007a).

Friddle, R., P. Podsiadlo, A. B. Artyukhin and A. Noy: Near-Equilibrium Chemical Force Microscopy. J. Phys. Chem. B., submitted. (2007b).

Green, N. H., P. M. Williams, O. Wahab, M. C. Davies, C. J. Roberts, S. J. Tendler and S. Allen: Single-molecule investigations of RNA dissociation. Biophys J **86**, 3811-21 (2004).

Heymann, B. and H. Grubmuller: Dynamic force spectroscopy of molecular adhesion bonds. Phys. Rev. Lett. **84**, 6126-6129 (2000).

Israelachvili, J. (1992). *Intermolecular and Surface Forces*. New York, Academic Press.

Johnson, K. L., K. Kendall and A. D. Roberts: Surface energy and the contact of elastic solids. Proceedings of the Royal Society of London, Series A **324**, 301-13 (1971).

Luan, B. and M. O. Robbins: The breakdown of continuum models for mechanical contacts. Nature **435**, 929-932 (2005).

Mate, C., G. McClelland, R. Erlandsson and S. Chiang: Atomic scale friction of a tungsten tip on a graphite surface. Phys. Rev. Lett. **59**, 1942-1945 (1987).

Merkel, R., P. Nassoy, A. Leung, K. Ritchie and E. Evans: Energy landscapes of receptor-ligand bonds explored with dynamic force spectroscopy. Nature **397**, 50-53 (1999).

Meyer, G. and N. M. Amer: Novel optical approach to atomic force microscopy. Appl. Phys. Lett. **53**, 1045-7 (1988).

Noy, A., C. D. Frisbie, L. F. Rozsnyai, M. S. Wrighton and C. M. Lieber: Chemical Force Microscopy - Exploiting Chemically-Modified Tips to Quantify Adhesion, Friction, and Functional-Group Distributions in Molecular Assemblies. J. Am. Chem. Soc. **117**, 7943-7951 (1995).

Noy, A., D. Vezenov and C. Lieber: Chemical Force Microscopy. Ann. Rev. Mat. Sci. **27**, 381-421 (1997).

Noy, A., D. V. Vezenov and C. M. Lieber (2007). Chemical Force Microscopy: Nanoscale probing of fundamental chemical interactions. *in Handbook of Molecular Force Spectroscopy*. A. Noy, Ed. New York, Springer**:** 97-122.

Patel, A. B., S. Allen, M. C. Davies, C. J. Roberts, S. J. B. Tendler and P. M. Williams: Influence of architecture on the kinetic stability of molecular assemblies. Journal of the American Chemical Society **126**, 1318-1319 (2004).

Pope, L. H., M. C. Davies, C. A. Laughton, C. J. Roberts, S. J. Tendler and P. M. Williams: Force-induced melting of a short DNA double helix. Eur Biophys J **30**, 53-62 (2001).

Rigby-Singleton, S. M., S. Allen, M. C. Davies, C. J. Roberts, S. J. B. Tendler and P. M. Williams: Direct measurement of drug-enzyme interactions by atomic force microscopy; dihydrofolate reductase and methotrexate. J. Chem. Soc.-Perk. Trans. 21722-1727 (2002).

Sinniah, S. K., A. B. Steel, C. J. Miller and J. E. Reutt-Robey: Solvent Exclusion and Chemical Contrast in Scanning Force Microscopy. J. Am. Chem. Soc. **118**, 8925-8931 (1996).

Skulason, H. and C. D. Frisbie: Rupture of hydrophobic microcontacts in water: Correlation of pull-off force with AFM tip radius. Langmuir **16**, 6294-6297 (2000).

Skulason, H. and C. D. Frisbie: Contact Mechanics Modeling of Pull-Off Measurements: Effect of Solvent, Probe Radius, and Chemical Binding Probability on the Detection of Single-Bond Rupture Forces by Atomic Force Microscopy. Analytical Chem. **74**, 3096-3104 (2002).

Strunz, T., K. Oroszlan, R. Schafer and H. J. Guntherodt: Dynamic force spectroscopy of single DNA molecules. Proc. Natl. Acad. Sci. USA **96**, 11277-11282 (1999).

Sulchek, T., R. W. Friddle and A. Noy: Strength of Multiple Parallel Biological Bonds. Biophys. J. **90**, 4686-4691 (2006).

Sulchek, T. A., R. W. Friddle, K. Langry, E. Y. Lau, H. Albrecht, T. V. Ratto, S. J. DeNardo, M. E. Colvin and A. Noy: Dynamic force spectroscopy of parallel individual Mucin1-antibody bonds. Proc. Natl. Acad. Sci. USA **102**, 16638-16643 (2005).

Sulchek, T. A., R. W. Friddle and A. Noy (2007). Counting and breaking single bonds: Dynamic force spectroscopy in tethered sinbgle molecule systems. in *Handbook of Molecular Force Spectroscopy*. A. Noy, Ed. New York, Springer Science+Business Media.

van der Spoel, D., P. J. van Maaren, P. Larsson and N. Timneanu: Thermodynamics of Hydrogen Bonding in Hydrophilic and Hydrophobic Media. J. Phys. Chem. B. **110**, 4393-4398 (2006).

Vezenov, D. V., A. Noy and P. Ashby: Chemical force microscopy: probing chemical origin of interfacial forces and adhesion. J. Adh. Sci. Tech. **19**, 313-364 (2005).

Williams, P. M., S. B. Fowler, R. B. Best, J. L. Toca-Herrera, K. A. Scott, A. Steward and J. Clarke: Hidden complexity in the mechanical properties of titin. Nature **422**, 446-449 (2003).

Zepeda, S., Y. Yeh and A. Noy: Determination of energy barriers for intermolecular interactions by variable temperature dynamic force spectroscopy. Langmuir **19**, 1457-1461 (2003).

Figures

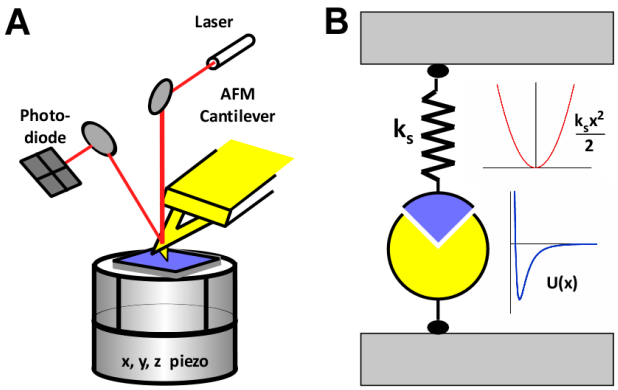

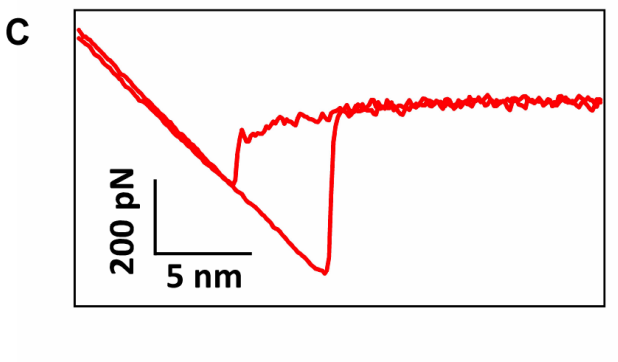

Figure 1. Measuring interactions forces with AFM cantilevers. **A.** Basic configuration of an atomic force microscope. B. A diagram of the force spectroscopy experiment showing the two main elements: a chemical bond and a loading spring. Insets show the potentials of the bond and the spring. **C**. A representative force vs. distance curve showing approach and retraction traces. The magnitude of the larger jump in the force-vs. distance curve measured the rupture (adhesion) force.

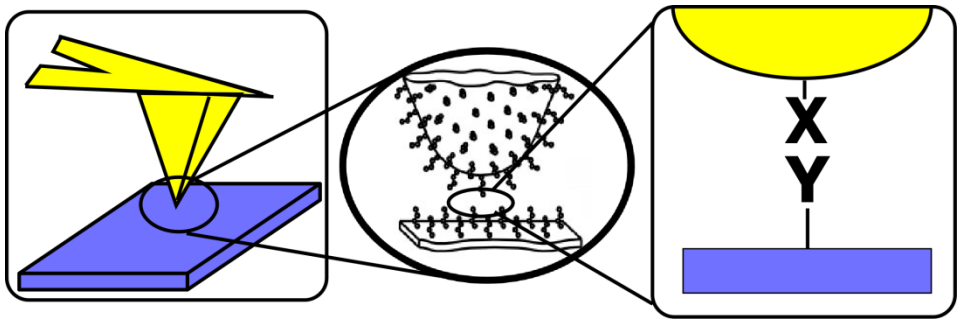

Figure 2. Basic principle of measuring intermolecular interactions using Chemical Force Microscopy. A probe tip of the AFM and a sample surface are modified with known chemical functionalities (typically using monolayers of long-chain organic molecules) to create a well-defined interaction in the tip-sample junction during the force measurement.

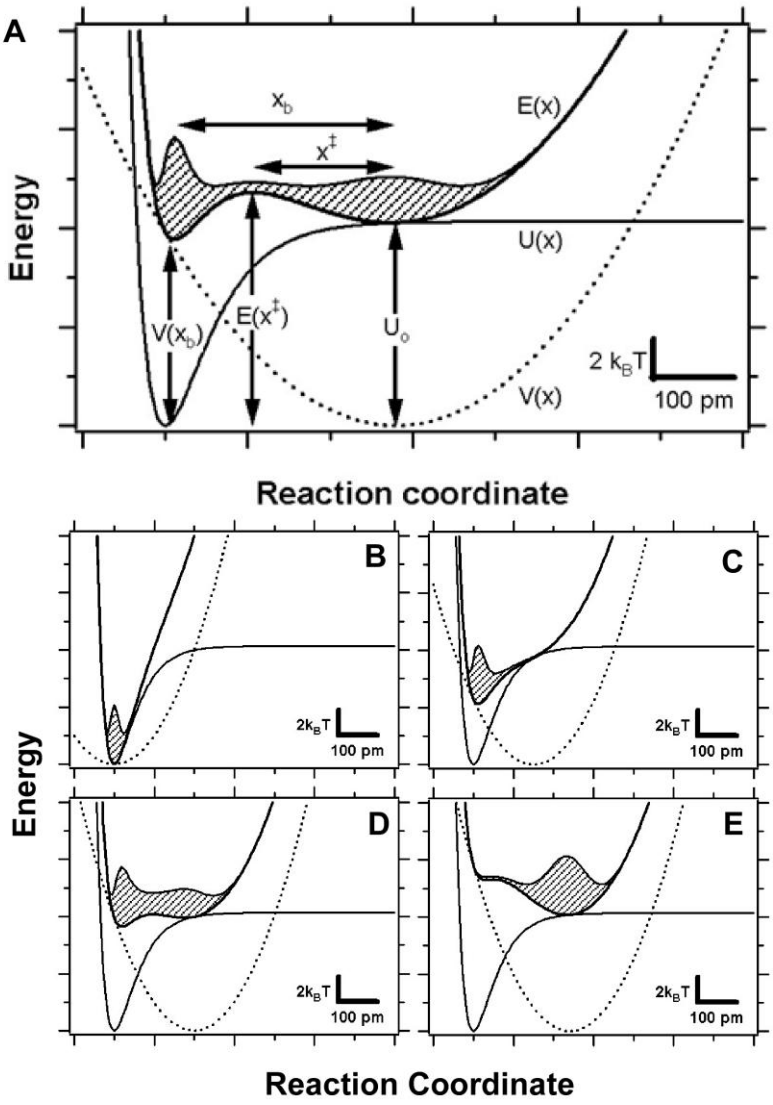

Figure 3. Potential energy surface for a typical force spectroscopy experiment. **A**. An interaction potential represented by the thin solid line loaded by a harmonic spring potential (dashed line). The overall potential energy profile of the system is shown by the thick solid line. The shaded area corresponds to the Boltzmann equilibrium density of states for that potential energy profile. (**B-E**). Snapshots of the potential energy surface during different stages of the numerical simulation of the loading process (Friddle et al., 2007b). The interaction potential used for these simulation was represented by a Morse potential $U(x) = U_0\left[1 - \exp\left(-2b\left(\frac{x}{x_0} - 1\right)\right)\right]^2$ with U_o=10·k_BT, x_o=1Å and b=1.0

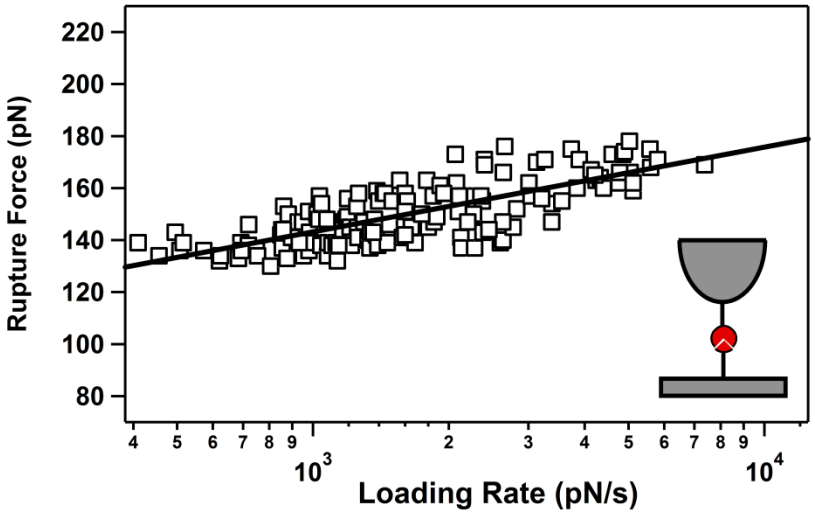

Figure 4. Force spectroscopy in the non-equilibrium regime. Dynamic force spectrum measured for an interaction of cancer marker Mucin-1 (MUC1) and a single-chain antibody fragment recognizing MUC1. Solid line corresponds to the fit top the data according to the Equation 4. Data from (Sulchek et al., 2005).

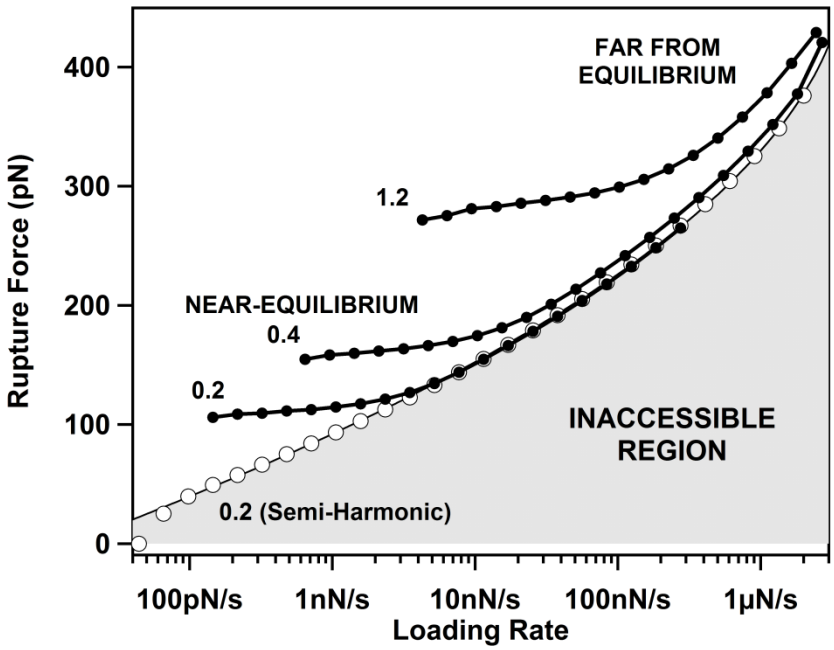

Figure 5. A "phase diagram" of a force spectroscopy experiment. Filled circles represent the force spectra showing loading of a Morse potential (see Figure 3 caption for the parameters) using harmonic cantilevers of different stiffness. A number next to each curve indicates the spring constant value used for the simulation. For comparison, open circles show a force spectrum calculated for a semiharmonic loading probe. Grey shaded region indicates a region of binding force and loading rate combinations inaccessible in the force spectroscopy measurements. From (Friddle et al., 2007b).

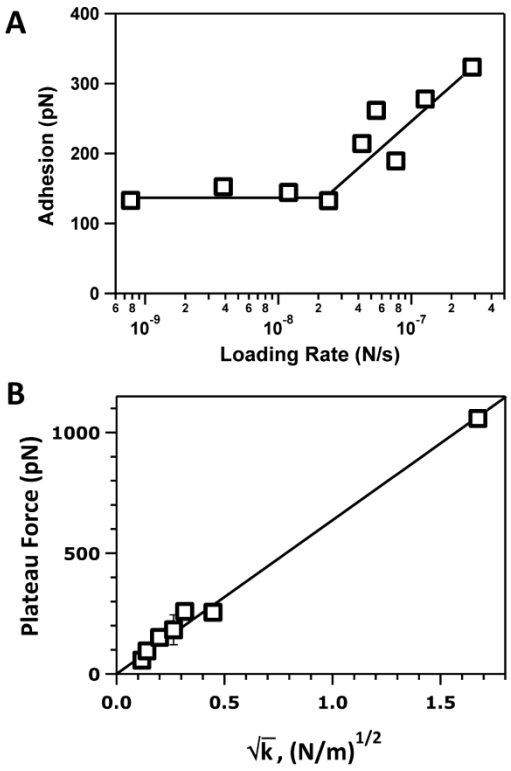

Figure 6. Force spectroscopy in the near-equilibrium regime. **A**. Dynamic force spectrum measured for interactions of a Au-coated probe tip and sample functionalized with COOH-terminated thiol molecules. Solid lines show the transition from a near-equilibrium to non-equilibrium unbinding regime. Data from (Zepeda et al., 2003). **B**. A plot of the measured equilibrium force plateau forces as a function of the cantilever stiffness used to collect the data. The solid line indicates the fit to the data according to the Equation 7. From (Friddle et al., 2007b).

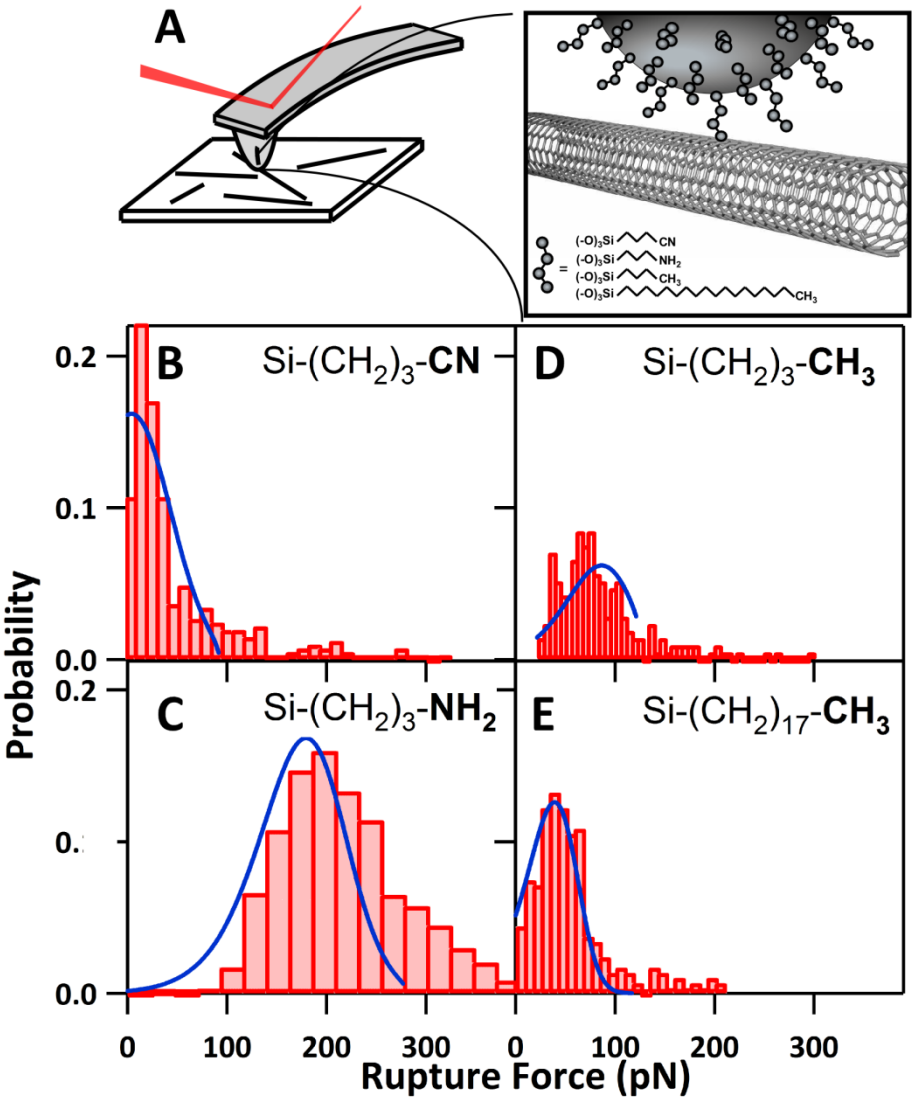

Figure 7. Chemical force microscopy of single functional group interactions with carbon nanotube sidewalls. **A**. A diagram showing the basic setup the experiment: a probe tip functionalized with silane monolayers terminating in a specific functionality contacts a highly-curved sidewall of an individual carbon nanotube. **B-E**. Histograms of the rupture forces measured with probe tips modified with (B) cyanopropylsilane, (C) aminopropylsilane, (D) n-butylsilane, and (E) octadecylsilane. Blue solid lines indicate the rupture force distributions predicted using Equation 8 and interaction potentials calculated by the *ab initio* simulations of functional group interactions with carbon nanotubes. A single damping coefficient value of $\gamma=3.5\cdot10^{-4}$ kg·s^{-1} was used to generate the calculated distributions on (B-D); a value of $\gamma=0.3\cdot10^{-4}$ kg·s^{-1} was used to generate the calculated distribution on (D). Data from (Friddle et al., 2007a).